Journal of Structural Geology, Vol. 9, No. 1, pp. 1 to 12, 1987
Printed in Great Britain

0191-8141/87$03.00 + 0.00

Deformation of the Assegaai supracrustals and adjoining granitoids, Transvaal, South Africa

C. J. TALBOT

University of Uppsala, Box 555, S-751 22 Uppsala, Sweden

D. R. HUNTER and A. R. ALLEN*

University of Natal, Pietermaritzburg 3200, South Africa

(*Received* 25 *April* 1985; *accepted in revised form* 4 *March* 1986)

Abstract—The structures in Archaean quartzites of the Assegaai greenstone belt in the Transvaal of South Africa can be interpreted in terms of three major deformation events. Earliest D_1 involved thrusting along brittle ramp and flat crush zones. Rising temperatures then led to the mobilization of SiO_2 and the development of syn-D_1 stylolites and omnidirectional quartz veins in the quartzites. Increasingly ductile behaviour results in some of the early D_1 crush zones being overprinted by late D_1 mylonitic shear zones while eastward-verging recumbent folds formed about N–S axes in the layered quartzites.

The Assegaai supracrustals were then separated from a contiguous basement of Ancient Gneiss Complex (AGC) by the intrusion of a granitoid sheet about 3 km thick along their sheared subhorizontal contact either late in D_1 or in the interval between D_1 and D_2. The supracrustals were then refolded about steep NNE-trending axial surfaces by concentric F_2 folds on a variety of scales. Such folds were the second major structures to affect the supracrustals but the first to deform the granitoid sheet.

The older of two suites of quartzo-feldspathic veins in the AGC were probably generated penecontemporaneously with the syn-D_1 quartz veins in ther Assegaai quartzites. This interpretation can be tested by removing the intense D_2 constriction (and 30% volume increase) recorded by a later network of syn-granitoid quartzo-feldspathic veins in the AGC from the $D_1 + D_2$ flattening recorded by the older veins. This procedure can be carried out by geometric vector subtraction on a Hsü diagram. The result reveals that the D_1 strains in the Assegaai supracrustals and the then contiguous AGC were identical penetrative subhorizontal flows prior to the intrusion of the intervening granitoid. The last significant strain in the region is represented by a brittle NNE-trending strike-slip fault and, locally in the quartzites, disharmonic conjugate folds.

INTRODUCTION

LIKE many Archaean greenstone belts elsewhere, the Assegaai supracrustal sequence (Fig. 1) is separated from orthogneisses nearby by a screen of post-greenstone intrusive granitoids (Hunter *et al.* 1983). The deformation of veins in the orthogneisses and quartzites in the Assegaai supracrustals is used here to establish the disposition of these two major rock suites when the granitoids were first intruded.

The orthogneisses, the two generations of veins found within them, and the intrusive granitoids are briefly described. The tectonic history is then reconstructed for those quartzites of the Assegaai supracrustal sequence exposed in the area shown in Fig. 2. Despite limited outcrop, the structural–metamorphic relations in the metamorphosed volcanics, pelites, banded iron formation and calc-silicates of the Assegaai supracrustal sequence further north are consistent with the same three deformation phases and two metamorphic events identified here (Hunter *et al.* 1983). The Assegaai supracrustals may be a dismembered extension of the southern portion of the Barberton greenstone belt exposed in the Motjane valley 75 km further north. The structural history interpreted here is similar to that reported in the Motjane valley by Jackson & Robertson (1983).

The intrusion of thin but extensive sheets of granitoid magmas along what were subhorizontal contacts between deformed or deforming covers and older sialic basements is becoming well established in the Archaean of southern Africa (Hunter 1957, 1968, 1973, Urie 1965, Jackson & Robertson 1983). A final discussion considers the role played by these granitoids during the development of the steep regional fabric considered characteristic of granite–greenstone belt terrains.

THE ANCIENT GNEISS COMPLEX

The gneisses at locality 3 (Fig. 1b) are bimodal in nature. Layered, medium-grained, leucotonalites to dark grey tonalites are interlayered with thin (*c.* 25 cm) plagioclase amphibolites with a pronounced foliation

* Present address: University College, Cork, Eire.

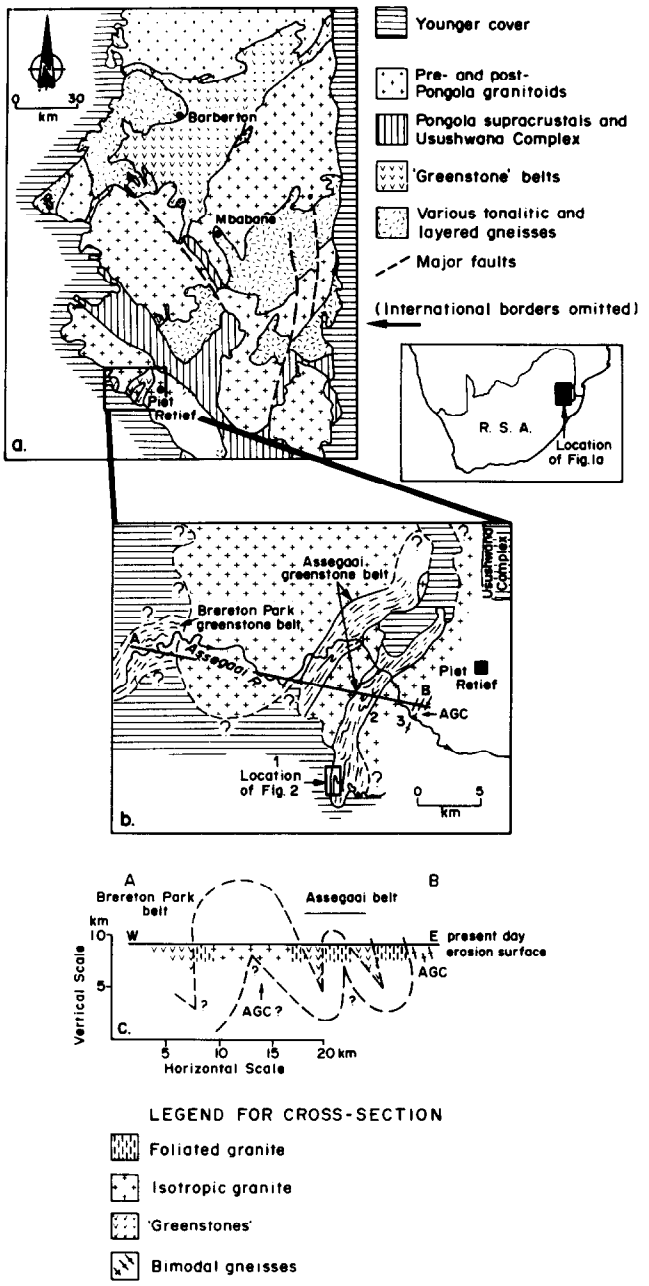

Fig. 1. The Assegaai 'greenstone belt' and its setting: (a) locality map; (b) simplified geological sketch map of the Assegaai supracrustal sequence showing locations discussed in the text; (c) simplified cross-section A–B.

subparallel to the lithological layering. These geisses are interpreted to be lateral equivalents of the bimodal suite of the Ancient Gneiss Complex (AGC) exposed over large areas to the northeast in nearby Swaziland (Hunter 1970, Jackson 1979, 1984).

The AGC in Swaziland is dominated by a bimodal gneiss suite comprising tonalite–leucotonalite and metabasite dikes. Both these components were apparently derived directly from the mantle at least 3.5 Ga ago and emplaced at hypabyssal or extrusive levels (Hunter *et al.* 1978). Between about 3.4 and 3.0 Ga ago they were strained repeatedly at depths ranging from about 20 km to within a few kilometres of the surface (Jackson 1984). We made no attempt to analyse the long and complex strain history within the AGC for it is sufficient for our limited purpose here to consider only those strains which affected the older of the two generations of quartzo-feldspathic veins within it.

Two generations of deformed quartzo-feldspathic veins are present in the AGC at locality 3 (Fig. 1b). Veins of the older generation are mainly of quartz but contain some microcline and albite and are characteristically a few centimetres thick.

The second generation of veins have a granodioritic composition and are composed of quartz, microcline–microperthite, plagioclase (An_{15-20}) and biotite. These veins range from a few centimetres up to ten metres in thickness and form an irregular network superimposed on both the lithological layering in the AGC and the older generation of thinner quartzo-feldspathic veins. The younger veins appear to represent a basal facies of the granitoid sheet immediately overlying the AGC in the west, but age relationships are not clear in the field. A casual inspection suggests that many are undeformed. However, a systematic study finds that folded examples cross-cut and post-date what appear to be thin straight 'undeformed' veins of similar composition. Close examination of such 'undeformed' veins disclose a crude foliation swinging around disaggregated feldspar megacrysts demonstrating that they have in fact been extended in subhorizontal sections (see later).

INTRUSIVE GRANITOIDS

A 3 km wide zone of granitoids intervenes between the easternmost Assegaai supracrustals and the AGC exposed still further east (Fig. 1b). A 2.5 km wide zone of similar granitoids occurs within the Assegaai supracrustals and a further zone, with a minimum outcrop width of 10.5 km, separates the Assegaai supracrustals from those of the Brereton Park area further west (Fig. 1b). These areas of granitoids are interpreted as antiforms of the same deformed sheet lying between the Assegaai supracrustals and the AGC. The geometry of this sheet is poorly known but probably had an original thickness of about 3 km (Fig. 1c).

Apart from the complex network of irregular cross-cutting veins of 'quartzo-feldspathic' granodiorite thinning downwards into the AGC from its base at locality 3 (Fig. 1b), this granitoid sheet is generally a medium- to coarse-grained leucotonalite (trondhjemite) composed of quartz, plagioclase and biotite, with minor amounts of microcline–microperthite. At locality 2 in Fig. 1(b), the upper part of the intrusion can be seen to have fed conformable sill-like sheets 1–5 m thick into the base of the supracrustals.

The granitoids, the Assegaai supracrustals and their mutual sheeted contact all share the same pronounced foliation and have obviously been deformed together. The foliation dips 75° ESE and is axial planar to subsimilar folds in layers of slightly more mafic mineralogy and a few quartzo-feldspathic veins in the leucotonalite within a few metres of its contact. The penetrative

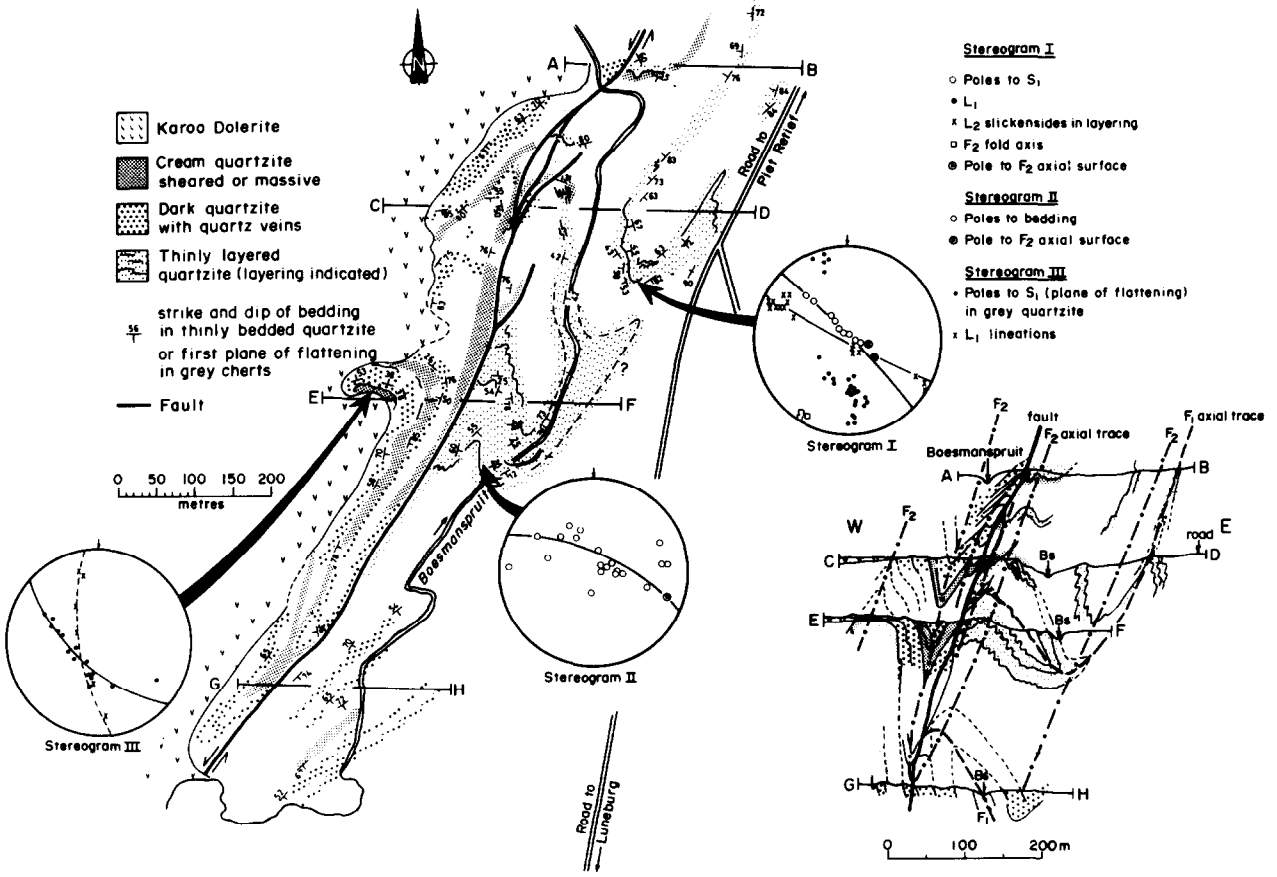

Fig. 2. Geological map, cross-sections and stereograms of location 1 outlined in Fig. 1(b).

foliation and the style of folding in the veins strongly suggest high-temperature solid-state flow after the leucotonalite intruded as a magma. Thin section examination confirms this interpretation but emphasizes that mylonitic deformation was superimposed later. The leucotonalite has a geometry similar to that of the sheet-like 3.0 Ga-old Lochiel granite exposed over large areas to the northeast.

Small bodies of pegmatitic granite within the Assegaai supracrustals are thought to be related to nearby pegmatites containing beryl, monazite and other exotic minerals (Hunter *et al.* 1983). If so, a minimum age for the leucotonalite is set by the date of 2.96 Ga obtained on a monazite from one such pegmatite (Burger & Coertze 1973).

DEFORMATION HISTORY OF THE SUPRACRUSTALS

Field and microscopic evidence indicate that the quartzites in the area illustrated in Fig. 2 underwent a deformation history involving two phases of cataclasis, faulting and SiO_2 mobilization (during early D_1 and D_3) with two intervening episodes of ductile strain (during late D_1 and D_2). These in turn were punctuated by the intrusion of the granitoid sheet (during late D_1 and/or D_2). Notice that the numbering of the deformations used here starts with the earliest deformation recognized in the supracrustals and neglects any preceding events in the AGC. Notice also that three phases of D_1 are distinguished (as early D_1, D_1 and late D_1) because they are considered to be separable phases of essentially the same progressive strain.

Early D_1*: ramp and flat crush zones in the quartzites?*

The earliest structures recognizable in the quartzites are localized zones of brecciation which reduced some of the thinly layered quartzites to the cataclastic precursor of the massive cream quartzites. Such early cataclasites are relatively easily distinguishable within the disorganized metre-sized blocks forming part of a much later zone of brecciation along a NE-trending fault (e.g. just SW of locality Y in Fig. 3).

Although the layering in the least broken rocks is now refolded by recumbent folds (Figs. 2 and 5), it is inferred to have been subhorizontal when parts of the sequence underwent early D_1 cataclasis. The early cataclasis occurred along mappable zones which may be either conformable or disconformable and curved (see the ornament for the sheared cream quartzite between the locations of sections EF and GH on the map of Fig. 2). Such subhorizontal and listric zones of cataclasis suggest the activity of early D_1 faults with flats and ramps.

Syn-D_1 *mobilization of* SiO_2

The effects of early D_1 cataclasis in the quartzites were subsequently overprinted and largely obliterated by

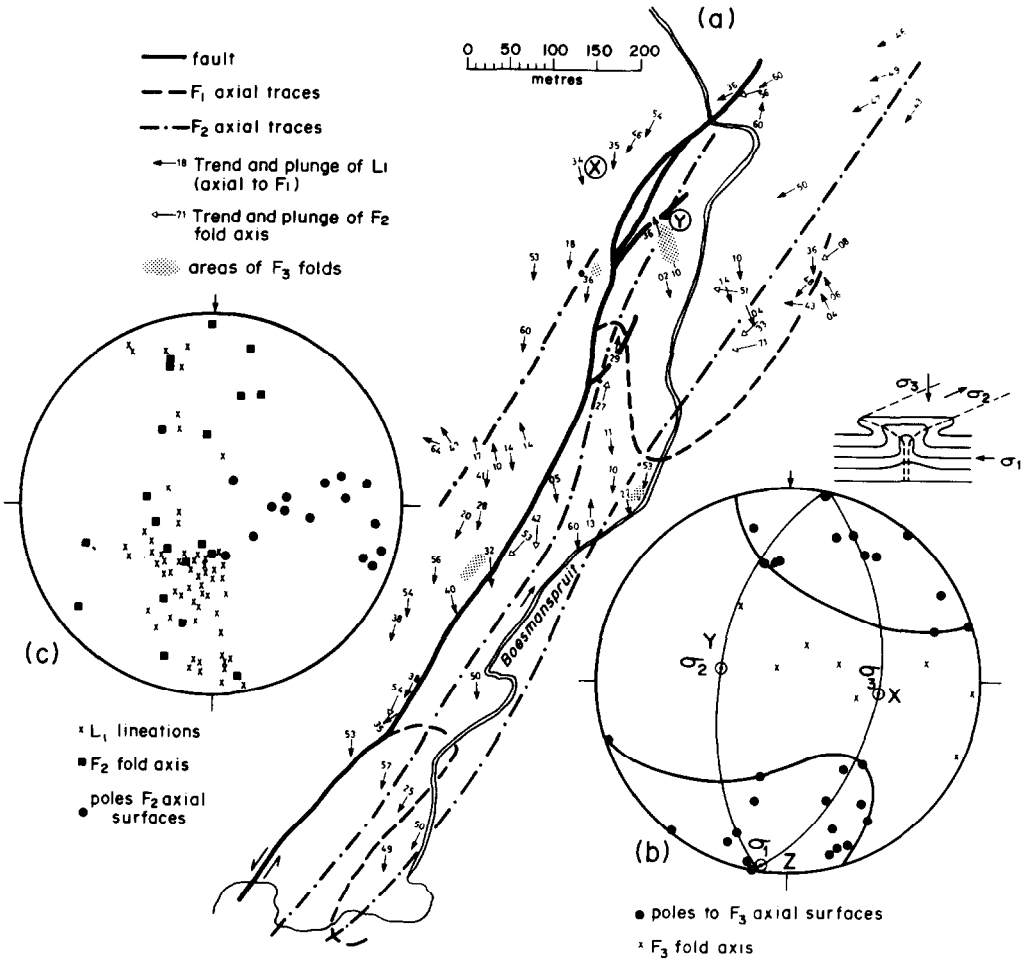

Fig. 3. (a) Map showing axial traces and lineations at location 1; (b) stereogram of poles to F_3 axial surfaces and fold axes; (c) stereogram of L_1 lineations, F_2 fold axes and poles to F_2 axial surfaces.

more ductile processes. These resulted in a pervasive grain shape fabric (S_1) and lineation (L_1) sub-parallel to the layering (bedding? see Fig. 3). The transition from early D_1 cataclasis and faulting to more ductile flow during late D_1, was accompanied, perhaps even ushered in, by a rise in temperature and a mobilization of SiO_2 in solution. This is when omnidirectional quartz veins developed in the dark ferruginous quartzites. Early stylolites in the quartzites indicate that at least some of the quartz in these veins was derived from the levels now exposed. (Later analysis will indicate that the oldest generation of quartzo-feldspathic veins in the then contiguous AGC developed slightly earlier.)

Late D_1*: recumbent folds and shear zones*

Late in D_1, the layering, S_1 and L_1, were all folded in some of the thinly layered quartzites by similar-type folds on a variety of scales. However, in other outcrops of the same rocks, L_1 can be seen to be axial to minor non-cylindrical F_1 folds even where these curve through 80° in a distance of a metre. L_1 from the whole of the area shown on the map (Fig. 2) clusters in the SSW quadrant but also lies in a partial great circle girdle trending N–S because of refolding by D_2 (Fig. 3c).

Minor isoclinal F_1 folds (Fig. 5) are refolded in several of the F_2 hinges exposed close to where the line of section CD is drawn in Fig. 2. A thin section perpendicular to the axis of such an F_1 fold shows quartz grains previously elongated parallel to the layering intensely buckled about the axial plane in the F_1 hinge (Fig. 4c).

The major F_1 folds interpreted in the thinly layered quartzites in sections A–H in Fig. 2 are confirmed by reversals of both S_1/layering and minor F_1 fold vergences. The major folds have limb lengths of at least 200 m even after the E–W shortening due to F_2. They therefore represent a major deformation involving large E-verging F_1 recumbent folds (section EF, Fig. 2).

The main expression of the late ductile phase of D_1 in the dark quartzites is the deformation of the quartz veins (e.g. Fig. 4b). S_1 in the dark quartzites is locally mylonitic where it overprints parts of the early D_1 zones of cataclasis (not illustrated). Such local mylonites indicate ductile shear zones which, during late D_1, acted as more penetrative versions of the preceding D_1 flat and ramp crush zones.

D_2 *in the quartzites*

F_2 folds ranging in wavelength from about 1 to 300 m are very obvious in the thinly layered quartzites. The axial surfaces of F_2 dip between 10 and 90°, mainly W

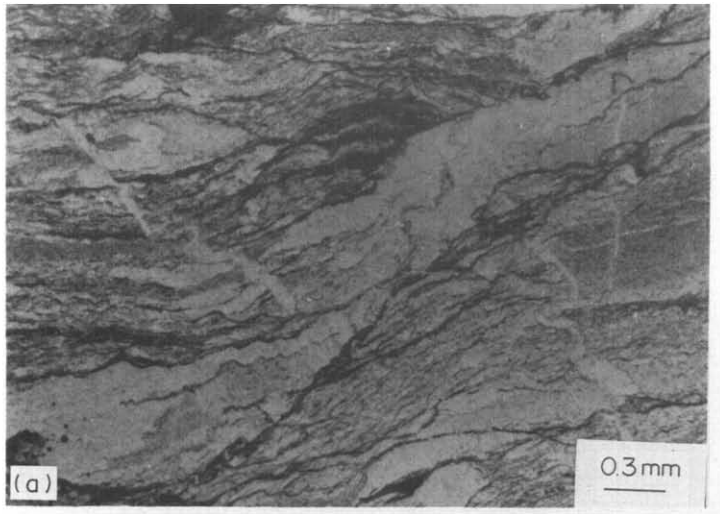

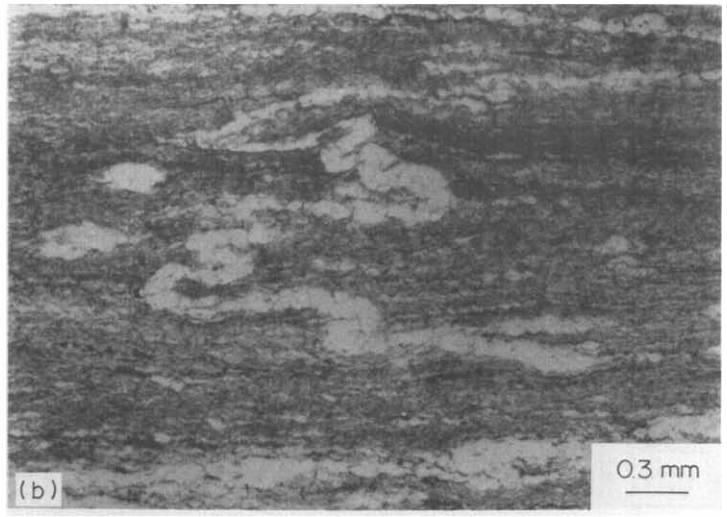

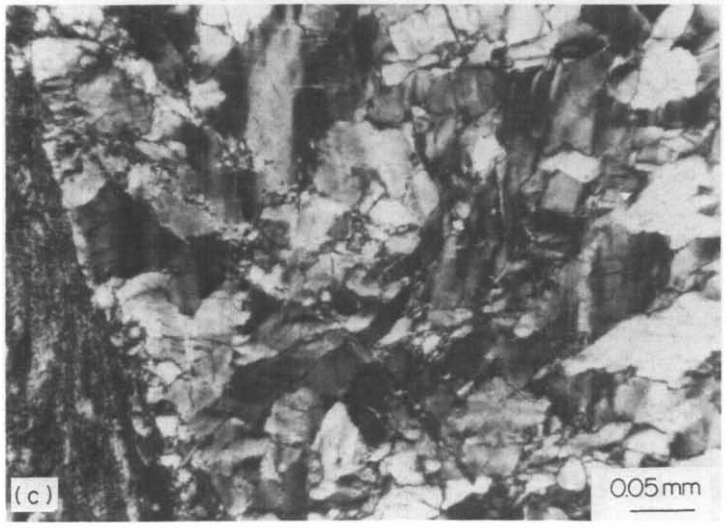

Fig. 4. (a) Photomicrograph of micaceous quartzite showing the crenulated foliation, folded quartz veinlets and stylolites (or tectonic stripes), plane polarized light; (b) photomicrograph of dark quartzite showing the S_1 foliation axial planar to folded quartz veins (plane polarized light); (c) photomicrograph of quartz fabric in the thinly layered quartzites in the hinge of an F_1 fold. A granular vein to the left parallels the axial surface of the fold. Note the intense kinking of the quartz grains parallel to the S_1 axial surface (crossed nicols).

Fig. 5. Photograph of minor recumbent F_1 fold refolded about a steep F_2 axial surface near the locality described by stereogram 1 in Fig. 2 (pencil about 14 cm long).

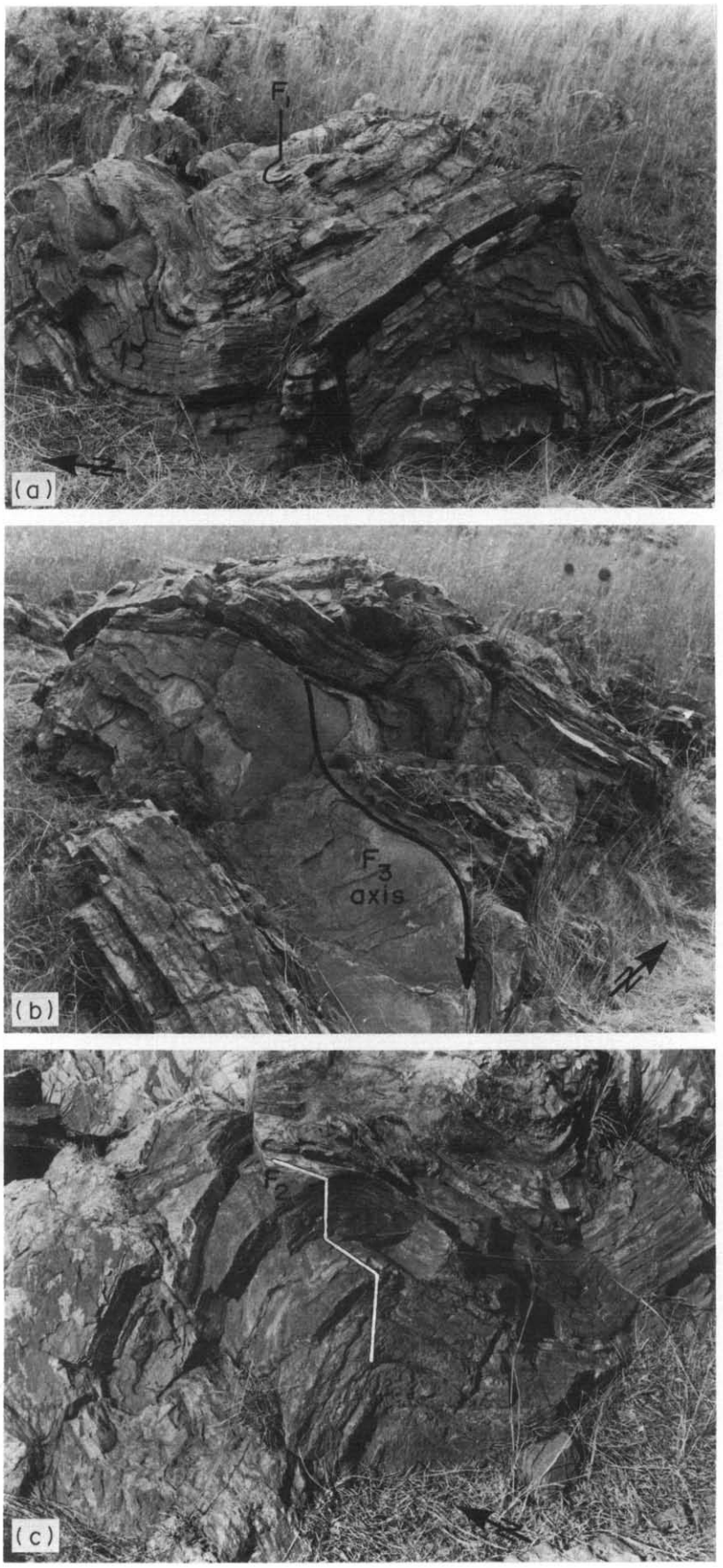

Fig. 6. Photographs taken from different viewpoints of the same outcrop about 1 m high (locality Y at north end of Fig. 3) in which all three generations of folds interfere in the same thinly layered quartzite; notice L_1 on all exposed layers. (a) A general view of the outcrop looking east showing refolding of a recumbent F_1 fold (arrowed). (b) An F_1 fold refolded by F_2 and F_3. The F_3 axis labelled displays variation in plunge due to the effects of F_2. (c) A steep F_2 axial surface.

and NW (Fig. 3c). The style of the F_2 folds in the thinly banded quartzites is concentric without any development of an axial-planar foliation. Instead, F_2 buckling of the thinly layered quartzites resulted in slip along the layering and the local development of slickensides subparallel to S_1 containing L_1 (e.g. stereogram 1, Fig. 2).

F_2 fold hinges lie in a broad girdle trending NNE (stereogram c in Fig. 3). This wide variety of plunges results from variations in the attitudes of the layering and S_1 due to the earlier effects of D_1. L_1 is folded about F_2 fold hinges (Figs. 3 and 6); stereogram 1 in Fig. 2 illustrates a particular example where L_1 lies in a partial cone with a 48° apical angle about the F_2 fold axis.

No minor F_2 folds were observed in either the massive cream quartzites or the dark quartzites. However, macroscopic F_2 fold closures (Fig. 2) and the localized development of a spaced (pressure solution?) cleavage in the former, and the deformation of the quartz veins in the latter (see below), illustrate that these lithologies were also deformed during D_2.

D_3 *in the quartzites*

Minor disharmonic folds or kinks are developed in small areas of the thinly layered quartzites (indicated on the map of Fig. 3). Some such folds are small individual buckles confined to only a metre or so of the sequence; these have axial surfaces perpendicular to the unfolded layering nearby. In other cases the axial surfaces of such buckles were nucleated in one layer, extend a few decimetres perpendicular to the layering and then curl in to parallelism with the layering a few metres away. Locally, pairs of axial surfaces to S and Z folds or kinks curve from the same point to define disharmonic box folds (see sketch insert by stereogram b in Fig. 3).

Stereogram b in Fig. 3 illustrates the range of orientation of F_3 axial surfaces. By analogy to laboratory experiments (Paterson & Weiss 1966), such folds relate to the principal stress field as shown in the diagram beside stereogram b in Fig. 3. Accepting this picture allows the definition of the principal stress field ($\sigma_1 \geqslant \sigma_2 \geqslant \sigma_3$) when the F_3 conjugate folds developed. F_3 fold axes lie in the layering and, as this varied in orientation because of the combined effects of F_1 and F_2, the few F_3 fold axes measured lie in a broad partial girdle centred on the $\sigma_2\sigma_3$ plane (Fig. 3b).

The most significant structure attributed here to D_3 is the NE-trending fault exposed for at least 1 km of its length and bisecting the area shown in Fig. 2. Where they are exposed, the traces of this fault and its splays are marked by late quartz-cemented breccias in which the chaotic blocks consist of early D_1 cataclasites in the cream quartzites and late D_1 mylonites in the dark quartzites. The main displacement surface appears to be parallel to the axial surfaces of F_2 folds and the splays tend to coincide with F_2 hinges in the massive dark quartzites. However, because the stress field interpreted from the late conjugate folds (Fig. 3b) could also account for this brittle fault, we believe these two categories of structure developed essentially synchronously. Bearing in mind that none of the rocks exposed on either side of the fault match within the area shown in Fig. 2, the stress field in Fig. 3(b) suggests that this fault involved a sinistral strike-slip displacement of its rigid walls in excess of 1000 m.

METAMORPHISM IN THE SUPRACRUSTALS

Mineral assemblages in the Assegaai supracrustals a few kilometres north of the area shown in Fig. 2 indicate that temperatures increased from greenschist to amphibolite facies during D_1 (Hunter *et al.* 1983). Thus S_1 is defined in the pelitic schists by aligned laths of white mica, chlorite and/or biotite, and staurolite appears to have grown late in D_1. Garnet, staurolite and andalusite all grew synkinematically with D_2 and temperatures and pressures reached a post-D_2 peak of 550–600°C at 4 kb.

D_3 was accompanied by retrogression in lower greenschist facies. Staurolite, garnet, andalusite, biotite and tremolite all reacted to form chlorite, white mica, chloritoid and serpentine (Hunter *et al.* 1983). Late stylolites in some of the quartzites probably record the source of the quartz cement in the fault breccia.

DEFORMATION OF THE VEINS IN THE QUARTZITES AND AGC

The quartz veins in the dark quartzites and the two generations of quartzo-feldspathic veins in the AGC (early D_1 and pre-D_2) were all deformed as competent single layers when their country rocks were deformed. Those in attitudes such that they were shortened are folded; those in orientations such that they were extended are either straightened or necked. This allows separate study of the bulk strain ellipsoids recorded by each generation of veins using the approach advocated by Talbot (1970).

Field work suggested that the early generation of quartzo-feldspathic veins in the AGC (locality 3, Fig. 1b) were contemporaneous with the single set of quartz veins in the supracrustals (locality 1, Fig. 1b), and that both these vein sets predate the intrusion of the granitoid sheet. For this to be so, the two sets of veins, now 7 km apart, must have been in proximity prior to the intrusion of the intervening granitoid sheet. They could be expected, therefore, to record similar strain histories when the effects of the strains that followed the intrusion of the granitoid sheet were removed. This test of our working hypothesis assumes that the post-granitoid strains recorded in the AGC at locality 3 (Fig. 1b) also affected the supracrustals at locality X (in Fig. 3), 7 km to the southwest.

The bulk $D_1 + D_2$ *strain ellipsoid*

Figures 7(a)–(c) are plots on lower hemisphere equal angle projections of the poles to planar elements of veins in the dark quartzite (at locality X in Fig. 3) and in the

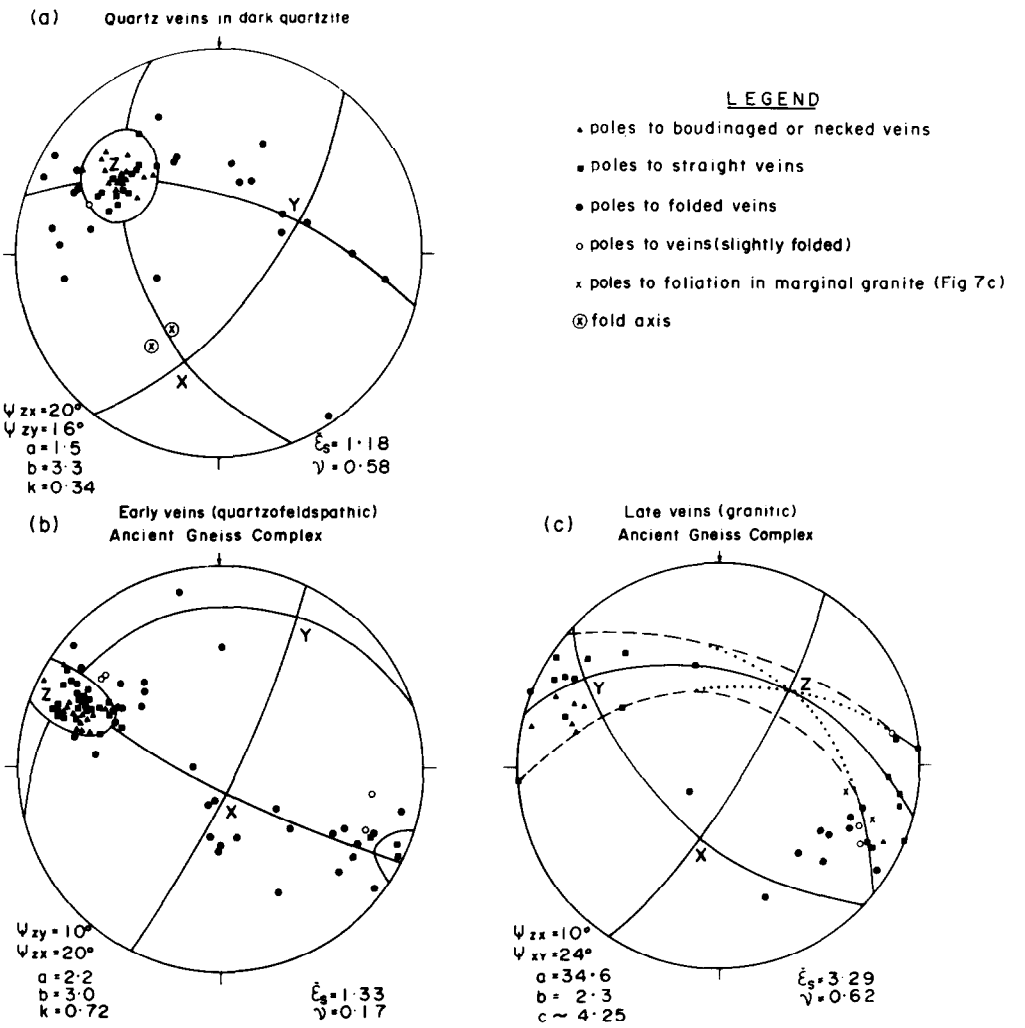

Fig. 7. Lower hemisphere, equal angle stereograms of strain data from locations 1, 2 and 3 indicated in Fig. 1(b). ψ_{zx}, ψ_{zy} and ψ_{yz} are the angular dimensions of the extension fields in the principal planes indicated (from Z, or, in the case of (c), Y, to the boundary). The axial ratios $a = X/Y$, $b = Y/Z$ and $k = (\ln a)/(\ln b)$ are listed at bottom left of each stereogram assuming no volume change (using Talbot 1970, fig. 5). Values for the natural strain $\bar{\varepsilon}_s$ and Lode factor ν (defined in the caption to Fig. 8) are listed bottom right of each diagram.

AGC (at locality 3 in Fig. 1). Such planar elements are parallel to the local fold- or boudin-envelope of any structures in the veins (Talbot 1970). Planar elements were distinguished as (clearly) folded, slightly folded, straight or necked in the field and are identified as such in Fig. 7. Talbot (1970) defined the area containing the poles to straight and necked competent veins on a stereogram as the field of overall extension. He showed that, for domains in which the bulk strain has been homogeneous, this field is elliptical, centred on Z and elongate in the ZX principal plane (where the axes of principal strain are $X \geq Y \geq Z$). All three sets of data in Fig. 7 are consistent with the picture that the veins were strained and rotated inhomogeneously on scales of centimetres or decimetres, but that these deformations can be integrated to allow the description of the ellipsoids of homogeneous bulk strain of the domains from which the data were collected (Talbot 1970). The approximate dimensions of the domains are 5 × 3 × 1 m in the dark quartzites (Fig. 7a) and 30 × 6 × 2 m in the AGC (Figs. 7b & c).

The elliptical fields of overall extension in Figs. 7(a) and (b) indicate that both the dark quartzites and the AGC are triaxially flattened, the dark quartzites rather more than the AGC. Poles to the 'straight' vein elements in Fig. 7c fall in an extension field wider than 105°. This is wider than theoretically possible in a homogeneously flattened rock complex (which would be a maximum of 90° without a volume increase larger than indicated). The data in Fig. 7(c) are therefore interpreted as an incomplete sample from a constricted rock complex.

The short but tightly constrained parts of the boundaries to the extension field (solid in Fig. 7c) were found empirically to extrapolate over the rest of the diagram as two great circles (dotted in Fig. 7c). These were first assumed to indicate a plane strain described by an extension field bound by circular sections intersecting at Z. However, if this were so, the extension field would have been a ZX line centred on Z (see Talbot 1970, fig. 4), but available data in Fig. 7(c) are more consistent with an intense and slightly triaxial prolate ellipsoid. In this case, the poles to 'straight' vein elements in Fig. 7(c)

should lie in a YZ girdle narrowest in ZX and widest in YZ (Talbot 1970). The two intersecting great circles were therefore modified as much as the data allowed to fit a pattern expected of a rock complex constricted homogeneously after the emplacement of the syn-granitoid veins. The result is an extension field which is constrained to within about 5° in the XY plane and poorly constrained in XZ (ψ_{zx} could be <10° but not much more), but is entirely consistent with what data there are in Fig. 7(c). Taking the dimensions of the extension field shown (ψ_{xy} = 24° and ψ_{xz} = 10°) implies an intense constriction with $a = 34.6$, $b = 2.3$ and $k = \ln a/\ln b = 4.25$, using formulae in Talbot (1970, p. 60) and assuming no volume change during the strain. Varying the values of ψ_{zy} and ψ_{xz} between the maximum ranges still consistent with the data makes surprisingly little change to the later manipulation. In fact it only decreases the volume change towards the values estimated in the field.

Removal of D_1 *from* $D_1 + D_2$

Strain data like those in Fig. 7 describe only minimum finite strain ellipsoids and, like all finite strain ellipsoids, are incapable by themselves of recording any information about their deformation paths. Thus the veins in the dark quartzites presumably strained differently during D_1 and D_2, but show no obvious signs of such a multi-phase history on either the outcrop or Fig. 7(a). This is because both strains must have been homogeneous on outcrop scale and the product of superimposing any number of ellipsoids is still merely another ellipsoid. However, the effect of D_2 is exclusively recorded by the second (syn-granitoid) generation of veins in the AGC (on Fig. 7c) and can be removed from the $D_1 + D_2$ strain ellipsoid recorded by the first generation of (pre-granitoid) veins in the AGC at the same locality (Fig. 7b). The data collection for Fig. 7(c) was deliberately restricted to the same rocks sampled in Fig. 7(b) for this purpose. The same D_2 strain can also be removed from the $D_1 + D_2$ strains recorded by the quartz veins in the dark quartzites about 7 km to the southwest (Fig. 7a).

For the sake of simplicity, the actual differences in the orientations of the principal axes of strain on Figs. 7(a)–(c) will be neglected and all three finite strain ellipsoids will be taken to be co-axial. This simplifying assumption allows the data to be shown and manipulated on the Hsü deformation diagram shown in Fig. 8 (Owens 1974). This diagram has the advantage over various adaptations of the Flinn plot (e.g. Flinn 1978, Talbot 1982) of showing the shapes, degree of distortion and orientation of co-axial ellipsoids in each of three potential orientations.

Owens (1974) has shown that volume change can be taken into account on a Hsü diagram by moving the central point (but see Flinn 1978). Only anisotropic volume changes can be accounted for with ease, but that is acceptable here when taking into account the 15–20% volume increase estimated in the field as a result of the emplacement of the second generation of quartzo-

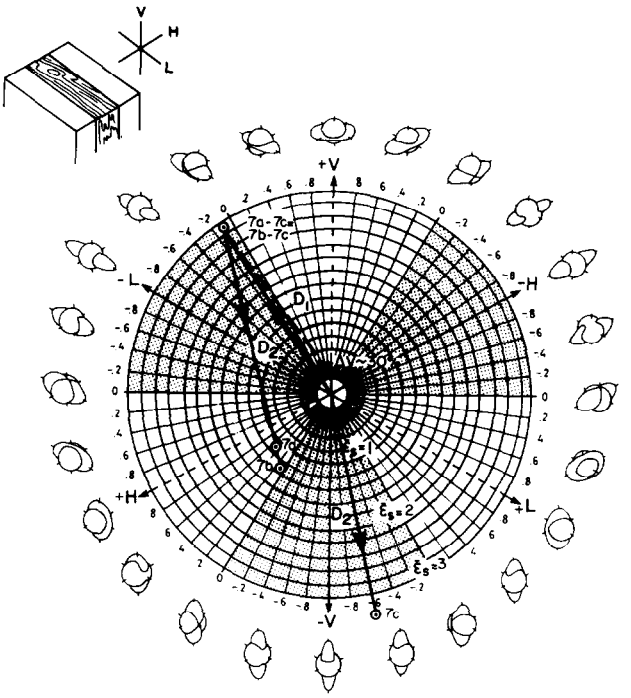

Fig. 8. Ellipsoids represented in Fig. 7 shown on a Hsü diagram appropriate for showing co-axial homogeneous ductile strains (Owens 1974, Hossack 1968). The orthogonal spatial axes (schematically related to the dominant deformation fabric of the Assegaai quartzites in the insert) are labelled H, L and V as proposed by Harland & Bayly (1958) when they suggested integrating contemporaneous minor structures and fabrics to assign the bulk strain of particular localities to one of thirteen potential tectonic regimes. In effect their suggestion is being followed here although not on the triangular diagram they advocated. This is because the simplest strain paths (when constant irrotational stress results in steady state co-axial irrotational strain, Ramsay 1967) have complex curved trajectories on the triangular plot but are straight radials on the Hsü diagram. The natural strain, $\bar{\varepsilon}_s$, is a measure of the distortion and increases linearly from the central point (representing a sphere).

$$\bar{\varepsilon}_s = (2/3)^{1/2}((\ln a)^2 + (\ln b)^2 + \ln a \cdot \ln b)^{1/2}$$ (Flinn 1978).

The Lode factor, ν, measures the shape of the ellipsoid,

$$\nu = \frac{\ln b - \ln a}{\ln b + \ln a}$$ (Flinn 1978)

and varies from 0 to +1 for oblate ellipsoids, and from 0 to −1 for prolate ellipsoids (which plot in the shaded segments); $\nu = 0$ for plane strains. Each of the six 60° segments bound by heavy radials (solid for −H, −V and −L and dashed for +H, +V and +L) are the equivalent of a simple Flinn diagram in that all possible ellipsoid shapes may be shown uniquely within each 60° segment if they have appropriate orientations (indicated by peripheral sketches). The D_2 vector to the ellipsoid represented by Fig. 7(c) has been removed from the $D_1 + D_2$ ellipsoids represented by Figs. 7(a) and (b) to reveal the D_1 vector. The D_2 vector removed from Fig. 7(b) includes a prolate volume increase of *c.* 30% due to the emplacement of the second generation of quartzo-feldspathic veins.

feldspathic veins into the AGC at locality 3 (Fig. 1b). This is because most of the second generation of veins (in Fig. 7c) now strike approximately NE (parallel to HL) so that the original volume increase they record can be assumed to have been essentially uniaxial prolate with X parallel to V (Fig. 8).

As a Hsü diagram defines a vector space, the effects of one strain superimposed on another can be removed by geometrical vector subtraction. Thus, in Fig. 8 the ellipsoid recording D_2 alone (Fig. 7c) has been removed from the two finite strain ellipsoids recording the combined

effects of $D_1 + D_2$ (Figs. 7a & b). This was done by removing the apparent strain path to the point representing D_2 in the AGC (Fig. 7c) from the point representing $D_1 + D_2$ in the dark quartzites (Fig. 7a) without any volume change, and from the point representing $D_1 + D_2$ in the AGC (Fig. 7b) taking into account a uniaxial prolate volume increase with X = V (see Fig. 8). The result demonstrates that, before D_2, the strains in the quartzites at locality X (on Fig. 3) and in the AGC at locality 3 (on Fig. 1) were identical in degree of distortion, shape and orientation if it is assumed that the proportional volume increase along X due to the emplacement of the second generation of quartzo-feldspathic veins in the AGC was about 30%.

The analysis illustrated on Fig. 8 demonstrates that, before the introduction of the syn-granitoid veins in the AGC, and before D_2, the earlier veins in both the supracrustals and the AGC recorded intense but almost plane strains ($\bar{\varepsilon}_s = 2.9$ and $\nu = -0.1$) with XY planes parallel to S_1 and HL, and X parallel to L. This is consistent with the earlier interpretation that the ductile phase of D_1 resulted in recumbent F_1 folds with L_1 statistically close to south-southwest trends in the supracrustals (Fig. 3c).

If the granitoid sheet intruded in the time interval between D_1 and D_2, then it can be expected to have had an isotropic fabric before D_2 and now to have a steep $L > S$ fabric as a consequence of the subsequent D_2 constriction. However, this is only consistent with initial reports (Hunter *et al.* 1983) that some of these granitoids have isotropic fabrics (on subhorizontal outcrops) if these are actually steep $L > S$ fabrics in three dimensions.

However, neither the Assegaai supracrustals, nor even the AGC at locality 3 (Fig. 1b), are characterized by $L > S$ fabrics. This is presumably because the D_2 constriction of these rocks was superimposed on already existing fabrics. An obvious inference is that more than just the top few metres of the granitoid sheet had a pre-exising late S_1 fabric. Further field work will be necessary to clarify whether the fabric in the granitoids involved constriction along or constriction superimposed on a pre-existing fabric.

The original vein patterns

Perhaps the most intriguing difference between Fig. 7(a) & (b) has not yet been alluded to. The poles to the veins cluster around the ZY plane in one, but the ZX plane in the other. The original attitudes of the veins in the AGC and the Assegaai quartzites must have been different. This presumably reflects different stress fields acting in these rocks when the veins developed.

The quartz veins in the dark quartzites (and the first generation of quartzo-feldspathic veins in the AGC) were irregular and branching, and had a wide range of initial orientations. The solutions responsible for both these veins and the contemporaneous early D_1 stylolites are therefore inferred to have dilated hydraulic brittle fractures in both extension and shear. Such a situation is

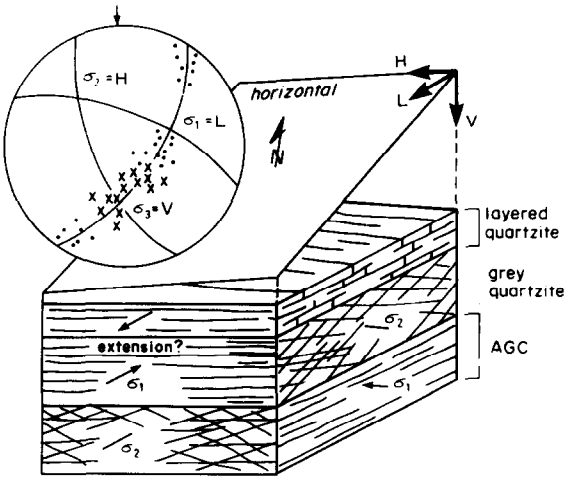

Fig. 9. Block diagram interpreting the pattern of quartz veins in the Assegaai quartzites and the pre-granitoid quartzo-feldspathic veins in the AGC in terms of different stress fields when they formed. The block is shown in its late-D_1 orientation. The stereogram illustrates what was probably the original disposition of the veins in the massive grey quartzites (with crosses being poles to veins infilling extension fractures and dots being poles to infilled shears).

only likely at depths deeper than a few kilometres (Roberts 1970). Poles to veins interpreted as dilating both shear and extensional fractures presumably clustered about σ_3 in the $\sigma_1\sigma_3$ plane (stereogram in Fig. 9). Taking account of the orientation of the vein patterns when they developed early in D_1 (Fig. 8), this assumption implies that σ_1 was subparallel to the subhorizontal contact between the AGC and the supracrustals as well as the fault flats in the supracrustals (Fig. 9). However, σ_1 trended NE in the supracrustals but NW in the deeper AGC (Fig. 9). A NE-trending σ_1 in the supracrustals, at a high angle to the ramps, suggests that the early D_1 crush zones in these rocks developed as a consequence of thrusting rather than extension (Fig. 9). Although it is not impossible, it seems unlikely that the subhorizontal WNW σ_1 implied by the original vein pattern in the AGC was contemporaneous with the ENE σ_1 inferred from the vein pattern in the cover (Fig. 9). Perhaps the first generation of veins in the basement slightly predated those in the cover.

In what could be the structurally highest quartzites (east of the late fault shown in Fig. 2), numerous thin quartz veins developed parallel to the layering while fewer and thicker (decimetre) examples originated perpendicular to the layering. These veins dilated only extension fractures suggesting that they developed in less deeply buried rocks extending in a SSW direction during early D_1 (Fig. 9).

DISCUSSION

Figure 10 summarizes in cartoon form on WNW–ESE sections a tectonic history consistent with the field observations, thin section studies and strain analyses presented here.

A similar tectonic history to the one interpreted here

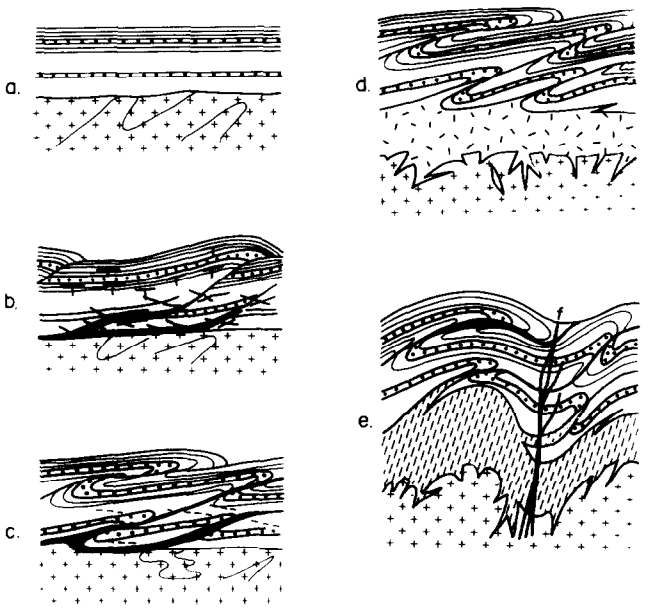

Fig. 10. Cartoon summary of the structural evolution of the Assegaai belt (not to scale). (a) Assegaai supracrustals (dots, clear and ruled) deposited on crystalline basement of AGC (crosses); (b) early D_1 local brittle deformation along ramp and flat crush zones (in black). Mobilization of SiO_2 indicated by stylolites and quartz veins in the cover and quartzo-feldspathic veins in the basement (short lines); (c) with increasing temperature, ductile deformation led to S_1 foliation in most of the supracrustals. Early crush zones were locally overprinted by mylonites (black) as E-verging folds resulted in recumbent nappes with N–S axes. Similar deformation of veins in both the dark quartzites and their basement indicates subhorizontal flow; (d) intrusion of granitoid sheet (random dashes with S_1 along top sheeted contact) along the sheared unconformity between the supracrustals and their basement. Top contact involved sills or apophyses of leucotonalite intruding the supracrustals while bottom contact was a network of granodioritic (quartzo-feldspathic) veins thinning downwards into the AGC; (e) D_2 refolding about NNE-trending axial surfaces in amphibolite facies. An S_2 fabric developed in the granitoid sheet (hatching) while S_1 was refolded by concentric folds in the quartzites. During later retrogression in the greenschist facies, a steep NNE-trending wrench fault (f) segmented the area while small disharmonic conjugate folds (not shown) developed locally in the thinly layered quartzites.

for the Assegaai area has recently been proposed for the Motjane schist salient of the Barberton greenstone belt 75 km to the north (Jackson & Robertson 1983). These authors interpret the Lochiel granite sheet as having been intruded along the contact between Archaean supracrustals and a basement of AGC after the supracrustal cover had already been deformed by recumbent folds and thrusts.

Jackson & Robertson (1983) distinguish several phases of the Lochiel granitoid sheet, but, despite reporting (p. 60) "the absence of D_2 folding predating the oldest neosomes", they argue that all phases were synkinematic with their D_2 event. This conclusion was based partly on evidence for progressive D_2 strain increments on successively younger veins being correlated with different phases of the Lochiel granite. Similarly, we have not recognized any signs of D_2 predating the granitoid sheet described here, but interpret this to indicate that this granitoid predates the whole of D_2.

Jackson & Robertson (1983) use the observation that the steep, weak foliation in the Lochiel granite is parallel to the foliation and bulk XY plane in the contiguous supracrustals as further evidence that the Lochiel granitoid sheet was synkinematic with D_2. However, the analysis of the strains in the Assegaai supracrustals and AGC offered here suggests that similar field relationships involved an early foliation in the siliceous metasediments (S_1) and an S_1 foliation in at least the top margin of the granitoid sheet as well. This foliation originally formed with a subhorizontal attitude and was only rotated to its present steep attitudes after intrusion of the granitoid sheet. If the magmatic intrusion of this leucotonalite sheet under the Assegaai supracrustals was synkinematic, it was late D_1 and not D_2.

The age relationship of the >2.96 Ga-old leucotonalite sheet described here to the 3.0 Ga-old potassic Lochiel granite is not clear. Dikes of potassic granite, which might be part of the Lochiel intrusive event, cross-cut leucotonalite 15 km northwest of the Assegaai supracrustal belt. It is therefore possible that the leucotonalites are significantly older than the Lochiel granite. The subtle differences in interpretation between that of Jackson & Robertson (1983) and that made here may therefore reflect similar events taking place at different times in nearby areas. This difference is worth resolving because it concerns whether the original magmatic intrusion or a later remobilization in the solid state imposed the steep dips considered characteristic of granite–greenstone terrains.

The 3.0 Ga-old Lochiel granite spread as a subhorizontal sheet less than 3 km thick between supracrustals and their gneissic basement over an area greater than 9000 km^2 (Hunter 1957, 1968, 1973, Urie 1965, Jackson & Robertson 1983). A similar but younger (2.7–2.4 Ga), thinner (*c.* 500 m) and less extensive (*c.* 1500 km^2) granitoid sheet separated the 2.9 Ga-old Pongola Supergroup from its underlying AGC basement in southern Swaziland (Hunter 1968, Jackson 1984). The intrusion of sheets of granitoids along the contacts between Archaean supracrustals and older gneissic basements is therefore well established in this part of southern Africa. We agree with the inference of Jackson & Robertson (1983) that the emplacement of these sheets as crystallizing melts is likely to have induced strains in both the granites and their country rocks. However, the vertical extension, lateral shortening, and steep D_2 foliation advocated by Jackson & Robertson (1983) would be very local and restricted to facies beside any thick margins of the spreading sheet. Lateral extension, subvertical shortening and a contact-parallel subhorizontal S_1 foliation would be far more general. The evidence presented here suggests that the original magmatic intrusion of the leucotonalite was synchronous with (and perhaps induced some of) the D_1 subhorizontal flow of its country rocks. Superimposition of the steep D_2 fabric was a later, separable event when the granitoid sheet was deformed in the solid state.

Acknowledgements—Harro Schmeling at Uppsala is thanked for his help in determining a and b from ψ_{xz} and ψ_{xy} for Fig. 7(c). Martin Jackson is thanked for criticism of, and Kersti Gløersen and Barbara Rimbault for typing, early versions of this work. Lesley Le Roux deserves special praise for her patient drafting of the figures. Field

accommodation was kindly provided by Texasgulf Exploration Limited. The award of a travel grant by the Council for Scientific and Industrial Research (CSIR) to C.J.T. was supplemented by the University of Natal. This, and financial support to D.R.H. for the continuing study of Archaean rocks in northern Natal and southeastern Transvaal by CSIR is gratefully acknowledged.

REFERENCES

Burger, A. J. & Coertze, F. J. 1973. Radiometric age measurements on rocks from southern Africa to the end of 1971. *Bull. geol. Surv. S. Afr.* **58**, 1–46.

Flinn, D. 1978. Construction and computation of three-dimensional deformations. *J. geol. Soc. Lond.* **135**, 291–305.

Harland, W. B. & Bayly, M. B. 1958. Tectonic regimes. *Geol. Mag.* **45**, 89–104.

Hossack, J. R. 1968. Pebble deformation and thrusting in the Bygdin area (S. Norway). *Tectonophysics* **51**, 315–339.

Hunter, D. R. 1957. The geology, petrology and classification of the Swaziland granites and gneisses. *Trans. Geol. Soc. S. Afr.* **60**, 85–125.

Hunter, D. R. 1968. The Precambrian terrain in Swaziland with particular reference to the granitic rocks. Unpublished Ph.D. thesis, University of Witwatersrand, Johannesburg.

Hunter, D. R. 1970. The Ancient Gneiss Complex in Swaziland. *Trans. Geol. Soc. S. Afr.* **73**, 107–150.

Hunter, D. R. 1973. The granitic rocks of the Precambrian in Swaziland. *Spec. Publs geol. Soc. S. Afr.* **3**, 131–145.

Hunter, D. R., Burker, K. & Millard, Jr., H. T. 1978. The geochemical nature of the Archaean Ancient Gneiss Complex and granodiorite suite, Swaziland: a preliminary study. *Precambrian Res.* **7**, 105–127.

Hunter, D. R., Allen, A. R. & Millin, P. 1983. A preliminary note on the Archaean supracrustal and granitoid rocks west of the Piet Retief. *Trans. Geol. Soc. S. Afr.* **86**, 301–306.

Jackson, M. P. A. 1979. High-strain deformation history of the Ancient Gneiss Complex in the Mankayane area, Swaziland: a preliminary account. *Geol. Soc. S. Afr., 18th Congr. Abstracts* **1**, 210–216.

Jackson, M. P. A. 1984. Archaean structural styles in the Ancient Gneiss Complex of Swaziland, southern Africa. In: *Precambrian Tectonics Illustrated* (edited by Kröner, A. & Greiling, R.). E. Schweizerbart'sche, Stuttgart, 1–18.

Jackson, M. P. A. & Robertson, D. I. 1983. Regional implications of early Precambrian strains in the Onverwacht Group adjacent to the Lochiel granite, north-west Swaziland. *Spec. Publs geol. Soc. S. Afr.* **9**, 45–62.

Owens, W. H. 1974. Representation of finite strain state by three axis planar diagrams. *Bull. geol. Soc. Am.* **85**, 307–310.

Paterson, M. S. & Weiss, L. E. 1966. Experimental deformation and folding in phyllite. *Bull. geol. Soc. Am.* **77**, 343–374.

Ramsay, J. G. 1967. *Folding and Fracturing of Rocks*. McGraw-Hill, New York.

Ramsay, J. G. & Huber, M. I. 1983. *The Techniques of Modern Structural Geology, Vol. 1: Strain Analysis*. Academic Press, London.

Roberts, J. L. 1970. The intrusion of magma into brittle rocks. In: *Mechanisms of Igneous Intrusions* (edited by Newall, G. & Rast, N.). *Geol. J. Spec. Issue* **2**, 287–338.

Smith, R. B. 1977. Formation of folds, boudinage, and mullions in non-Newtonian materials. *Bull. geol. Soc. Am.* **88**, 312–320.

Talbot, C. J. 1970. The minimum strain ellipsoid using deformed quartz veins. *Tectonophysics* **9**, 47–76.

Talbot, C. J. 1982. Obliquely foliated dykes as deformed incompetent single layers. *Bull. geol. Soc. Am.* **93**, 450–460.

Urie, J. G. 1965. Forbes Reef–Ngwenya iron mine area, Hhohho District. *A. Rep., Geol. Surv. Mines Dept, Swaziland*, 7–8.